FAILURE MECHANISMS IN FATIGUE OF FIBRE GLASS REINFORCED POLYAMIDE 6.6

J.A. Casado, F. Gutiérrez-Solana, J.A. Polanco and I. Carrascal

Laboratorio de Ciencia e Ingeniería de Materiales.
E. T. S. de Ingenieros de Caminos, C. y P. Universidad de Cantabria.
Avda. Los Castros s/n. 39005 - Santander (SPAIN)

ABSTRACT

In this work a characterisation of the mechanisms involved in the fatigue behaviour of a composite material with thermoplastic polymeric matrix is established. The material is a fibre glass reinforced polyamide 6.6 (PA 6.6) with 35% of short fibre uniaxially oriented, used in insulating joints of railway components.

Normalised tensile specimens were tested in tensile fatigue. The tests were carried out by using sinusoidal waves in load control at different stress levels and at room temperature. The humidity content in the material was 2%, corresponding to the equilibrium value raised after storage in the laboratory. From the tests on tensile specimens, the applied load and the strain have been continuously recorded in order to determine the evolution of the maximum strain and loss energy as an indicator of the material´s damage due to the fatigue processes. The evolution of temperature in the surface of the specimens with the number of cycles applied was also recorded to relate its influence in the coupled creep-fatigue effect that takes place in the fatigue tests. Also surface roughness measurements have been done to be correlated to the crazing distribution

Finally, the SEM fractographic analysis done on the fracture surfaces of the tested specimens has shown different features due to the different crack propagation mechanisms, that have been related with both the thermal and the loading histories of the material.

1 INTRODUCTION AND OBJECTIVES

The modern railway tracks used by high speed trains incorporate fastening elements which fix the rail in place, maintain the gauge and insulate electrically both rails. A sketch of a standard fastening system, named HM, is shown in Figure 1a, where all the different components are presented. There are two screws with their corresponding washers to connect the elastic metal springs to the rail. There is also a neoprene plate placed under the rail to absorb most of the vibrations produced by the passing of the trains and two polymeric parts, one on each side of the rail, to conserve constant the value of the gauge. A detail of the insulating polymeric part is presented in the picture of Figure 1b. An important cause of deterioration of the insulating fastening railway parts, injected with short fibre glass reinforced PA 6.6, is associated to dynamic mechanical fatigue process originated when the trains circulate through the line [1-3]. The thermoplastic material of the insulating parts is subjected to fluctuating loads whose periodical repetition produces its thermal heating, changing its flexibility and mechanical behaviour. Experimental laboratory techniques were used to reproduce the fractures found in the in-service parts [4], showing that the fracture was due to fatigue processes.

The aim of this work is to establish the failure mechanisms in fatigue of fibre glass reinforced polyamide 6.6 (PA 6.6) that establish the in service limit conditions of these high responsibility components, injected with this reinforced thermoplastic polymer.

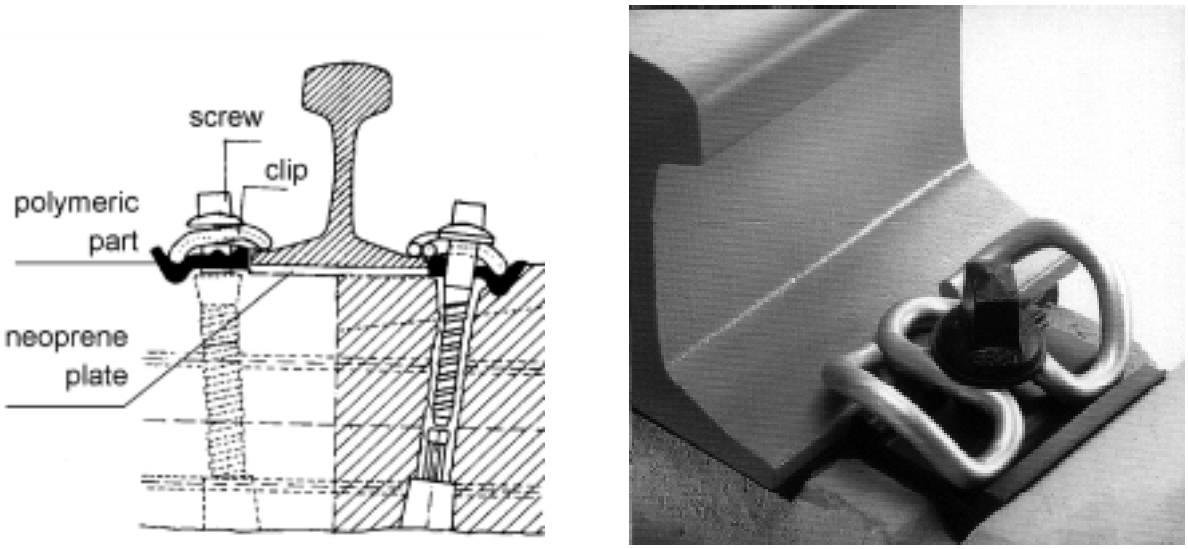

a: General sketch **b:** Detail

Figure 1: HM fastening.

2 MATERIAL TESTED AND EXPERIMENTAL TECHNIQUES

This work studies the tensile fatigue behaviour of PA 6.6, commonly known as “nylon”, reinforced with 35% of short fibre glass by weight. Normalised tensile strength specimens were used in accordance with the corresponding UNE standard [5]. They were made by injection moulding in such a way that the short glass fibres (150 μm length and 10 μm diameter) were oriented parallel to the longitudinal axis of the specimens. Notch and unnotch normalised tensile specimens were tested in tensile fatigue. The notchs on to the specimens were perform using a sharp knife blade fixed to an hydraulic machine´s grip. The specimens were placed in a base under the blade whose slow controlled advance produced the desired crack size of 2 mm depth in the material.

As a starting value, the strength (σ_r) was determined for the material under dynamic conditions by applying a tensile impact load onto the specimen, with the velocity given by the generation of a square wave form. The fatigue tests were performed on a universal mechanical testing machine under load control and at laboratory room temperature. The applied stress levels fall between a maximum (σ_{max}), variable from test to test, and a minimum value (σ_{min}) set at 0.05 σ_r, to avoid compression and possible specimen bending. The initial upper stress state was 0.90 σ_r. Each test was performed until the specimen broke. The value of σ_{max} was reduced test by test at intervals of 0.10 σ_r until the material withstood 10^6 cycles without breaking. The highest stress variation reached by this sequence was called $\Delta\sigma_6$. The tests were performed with sinusoidal load waves at a frequency of 5 Hz.

The following information was registered during the tests: applied stress variation; specimen´s temperature, using a thermocouple located on the surface of the specimen´s calibrated zone; variation in the length of the specimen´s calibrated zone using an extensometer; and the number of cycles withstood up to fracture. These measurements make it possible to continuously monitor the evolution of temperature and flexibility for each specimen during the test.

3 RESULTS AND ANALYSIS

The value of σ_r for the material studied under tensile impact conditions was 166.8 MPa, and the value of $\Delta\sigma_6$ obtained, which represent its resistance to fatigue, was 58.4 MPa (35% σ_r), corresponding to a σ_{max} of 0.4 σ_r.

Figure 2 shows the results obtained for the material under continuous fatigue with sinusoidal wave form. The graph represents the evolution of the material´s deformation versus the number of cycles applied, for the different stress levels considered.

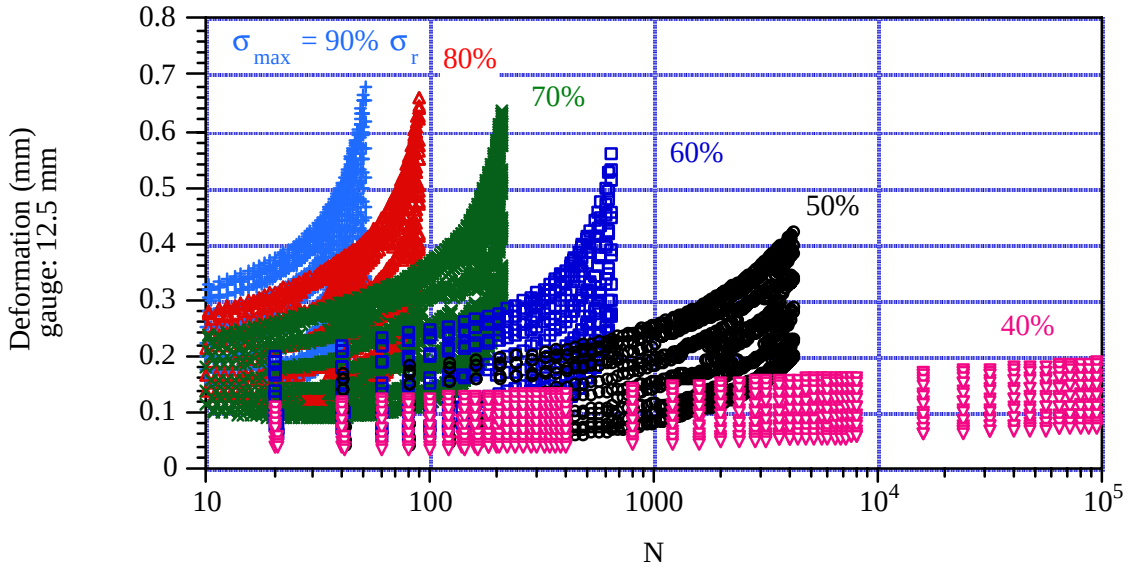

Figure 2: Material´s deformation evolution through all the tests.

Figure 3 shows, in a double plot both, the material´s deformation evolution, corresponding to the maximum of the peaks of the load waving, and the surface temperature versus the number of cycles applied, for each stress level considered. Both parameters, deformation and temperature, only stabilise at the loading level corresponding to $\sigma_{max} = 40\%\sigma_r$ [6].

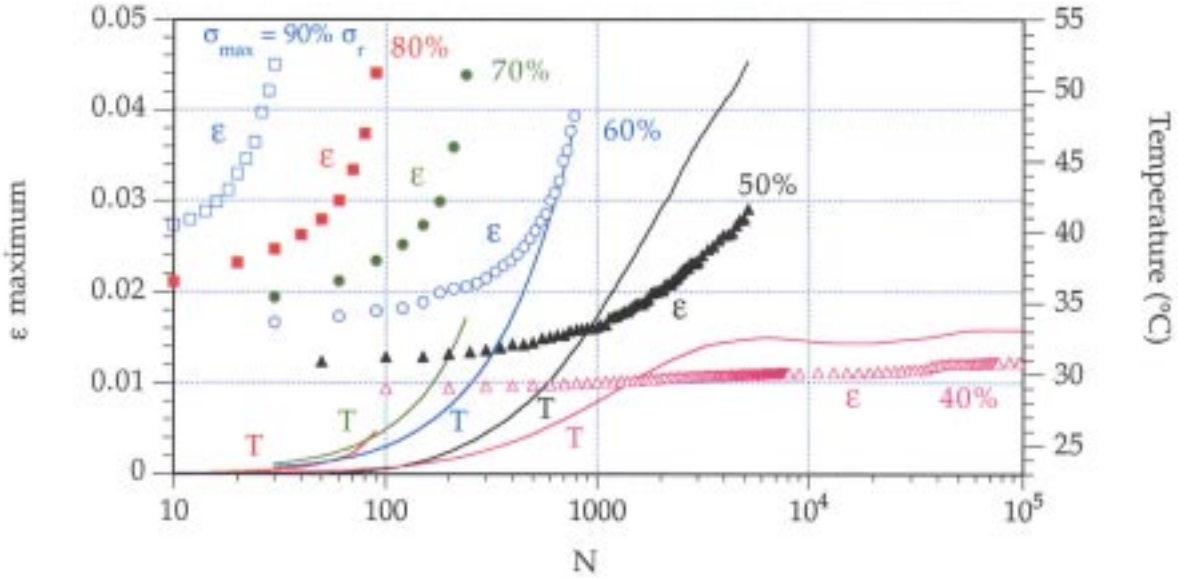

Figure 3: Material´s deformation evolution and temperature as a function of the number of cycles.

From the previous results, it is obtained the evolution of the deformation velocity as a function of loading cycles applied on to the specimens ($\partial\varepsilon/\partial N$) for all the stress levels considered, as Figure 4 represents. In this graph we can observe that for maximum loads bigger or equal to $60\%\sigma_r$, except for 90%, there is an initial decreasing in the deformation velocity reaching a minimum value. Then there is slow increase of this parameter until a critical condition is obtained, for which a rapid growth of deformation velocity takes place, preceding the final fracture. However, for loads equal or lower to $50\%\sigma_r$ the parameter ($\partial\varepsilon/\partial N$) remains apparently constant throughout the test. Then it is possible to establish two main transitions in the material during the dynamic process for each load level, for which some mechanical effects, thermally affected, take place. Therefore, three stages can be observed in the behaviour shown in Figure 4. They are pointed as I, II and III.

A parallel study was performed taking into account the material´s loss energy, i. e. hysteresis energy, during the tests [7]. The graph of Figure 5 shows the evolution of loss energy (E_H) for the material as a function of the number of cycles applied for each loading condition.

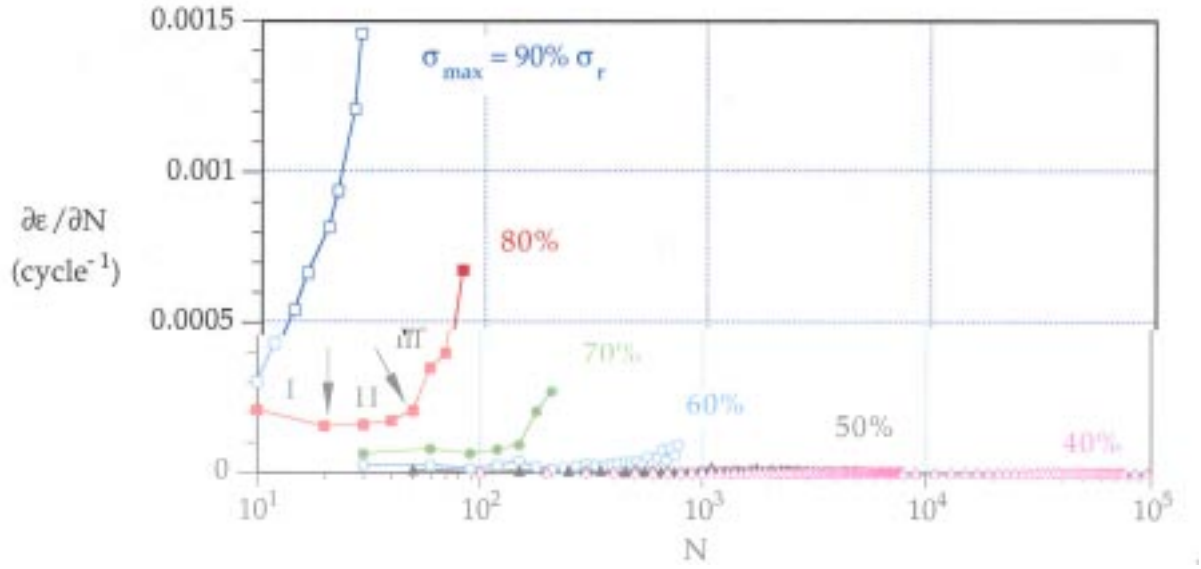

Figure 4: ∂ε/∂N = ∂ε/∂N (N)

The parameter E_H was measured considering the enclosed areas corresponding to the hysteresis loops obtained from the stress-strain registers throughout the tests. From these results the evolution of the loss energy velocity with the number of cycles ($\partial E_H/\partial N$) was determined and it is shown in the same graph of Figure 5. The shape of the evolution of E_H with N reassembles the one for ($\partial\varepsilon/\partial N$), meanwhile its derivate ($\partial E_H/\partial N$) shows, again, up to three main zones: a decreasing one (I) followed by a constant one (II) and finally a sharp increasing (III). These zones are pointed in Figure 5 for the loading condition $\sigma_{max} = 60\%\sigma_r$. Therefore, again two apparent transitions are observed in the material´s behaviour which coincide in the time with those previously defined for ∂ε/∂N.

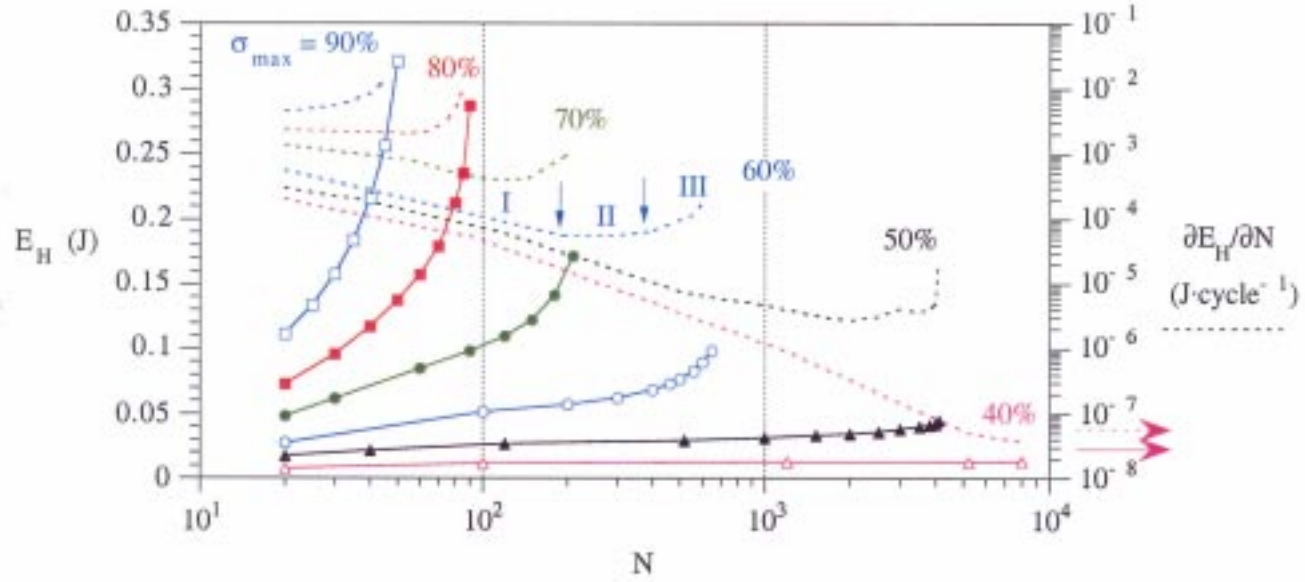

Figure 5: Absolute value and rate of energy loss per cycle.

Figure 6 presents the material´s surface temperature in relationship to the maximum of deformation experimented by the material during the tests obtained from Figure 3. In the same graph the conditions (ε, T) corresponding to the transitions observed in Figure 4 ($\partial\varepsilon/\partial N$) and Figure 5 ($\partial E_H/\partial N$), coincidents at each loading for both variables, are represented. For both conditions, the connection of all the transition points leads to the obtention of two constant strain lines (dashed and continuous) corresponding to values 2.2 ± 0.1 and $2.8 \pm 0.1\%$. No influence of temperature is observed for these transitions. These results agree with that obtain for the specimen tested up to 40% σ_r, i. e., the material didn´t break after been applied one million cycles, because it always maintained a deformation lower than that to change to stage II.

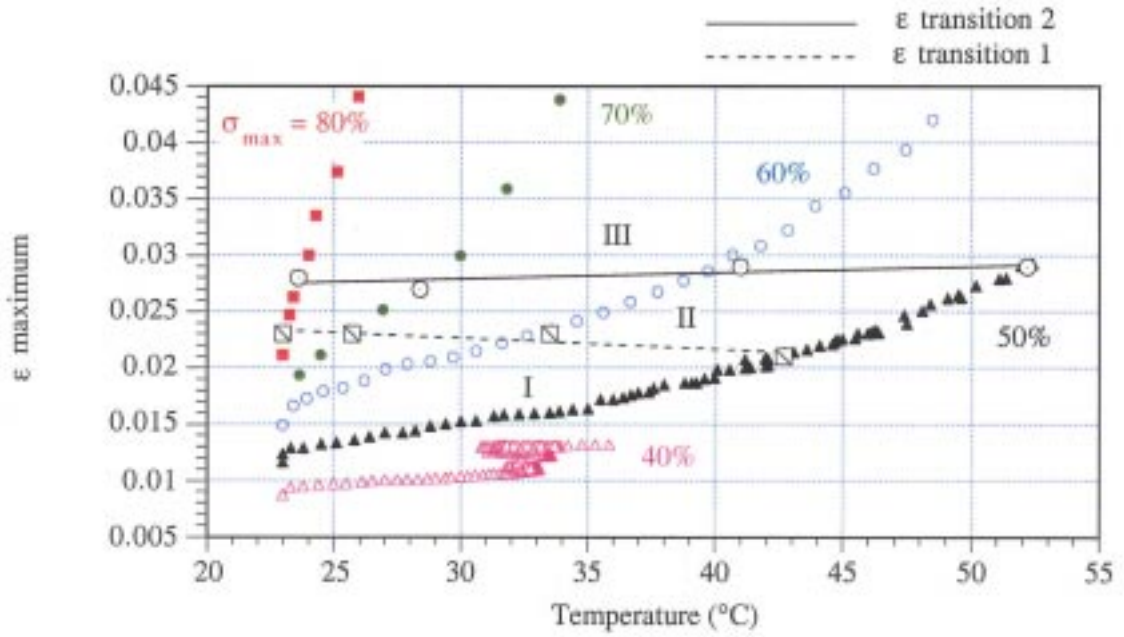

Figure 6: $\varepsilon_{max} = \varepsilon_{max}(T)$

After the tests the material´s fracture surface showed two different morphologies as can be observed in the scanning electron microfractographies of Figure 7.

The mechanisms leading to a final rupture can be established as follows:

- Once the first transition is reached the sample starts to generate crazing areas (stage II).

Then, when the second transition is reached, local instabilities are concentrated due to the crazes breakage, producing a crack (stage III) which becomes critical when the stress reached approaches the material´s strength. This value decreases with the increasing in temperature[6], which grows continuously during the test.

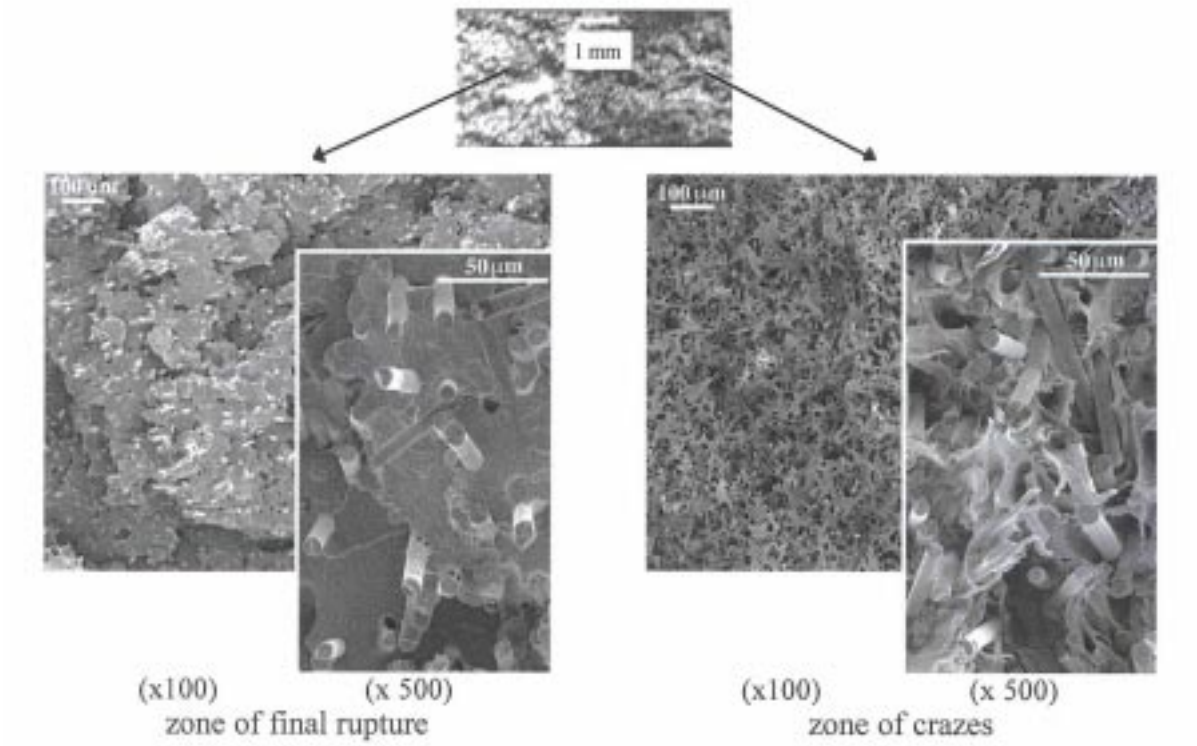

Figure 7: *Fractography of the fracture surface of one of the samples tested.*

The first statement, crazing mechanisms at stage II, has been pointed out by the surface roughness measurements [6]. This technique reveals that lateral surface roughness increases during the fatigue tests from a critical condition corresponding to the first transition. For the sample tested at $\sigma_{max} = 50\%\ \sigma_r$, Figure 8 shows this situation. The increase in surface roughness is associated to the growth of crazing areas emerging at the sample lateral surface. Finally, this lateral surface roughness measured under the fracture surface increases due to the unstable final process, i. e., at stage II.

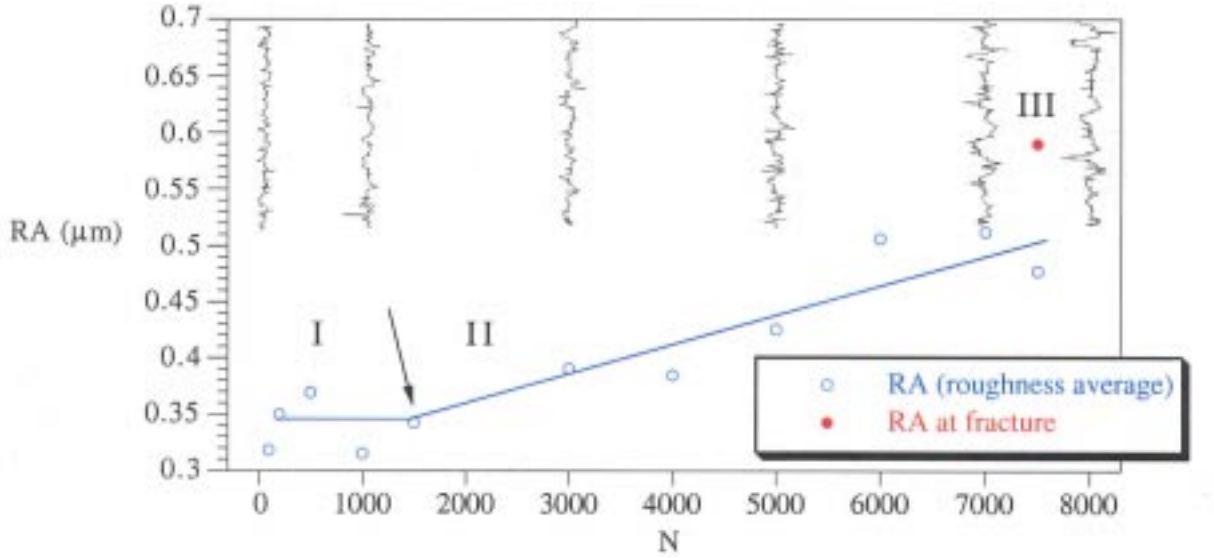

Figure 8: *Lateral roughness evolution of the sample tested at σ_{max} = 50% σ_r.*

To determine the conditions that establish the mechanisms transition and the corresponding critical states in the material to take into account the observed effect of increasing temperature, creep tests were carried out on the material at different temperatures. Figure 9 shows the strain evolution in the material for a stress applied of 83.37 MPa ($0.50 \cdot \sigma_r$) at 23, 28, 33, 38 and 43 °C.

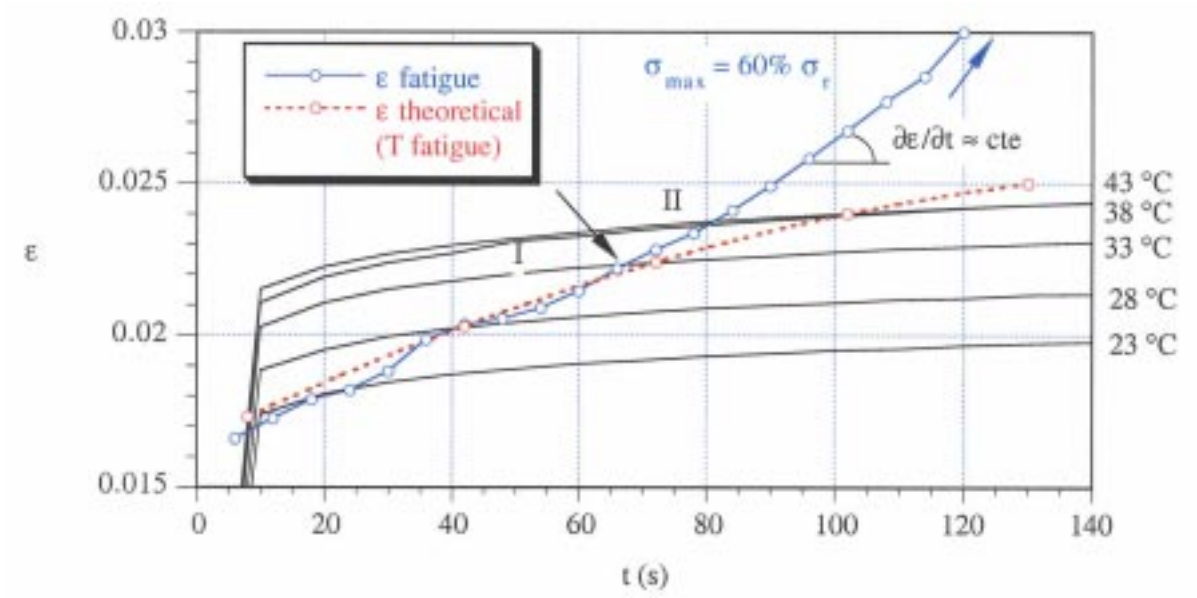

Figure 9: *Creep tests at different temperatures.*

In the same representation it can be seen in a dashed line the theoretical strain reached for the material during the fatigue test if it could be associated to a creep process only affected for the different thermal states reached during the dynamic test. For this theoretical approach it has been considered that the fatigue variable loading with σ_{max} = 60%σ_r has a creep effect equivalent to a constant load of 50%σ_r, based on the equal strain evolution at initiation of fatigue processes. Plotting in the same graph the experimental deformation obtained in the fatigue test, it is possible to verify the moment in which there is a divergence (indicated with an arrow) between the theoretical static behaviour and that produced by the fatigue process. This point refers to the same instant where the first critical transition (stage I to stage II) was found for the test under analysis. So, from now on, all the internal heat generated produces successive cohesive cracks or crazes that still are able to transmit some stress meanwhile the second transition is not reached.

Therefore, stage I behaviour is only associated to the creep behaviour of the material depending on loading and temperature evolution due to fatigue. This justifies the decreasing value of $\partial\varepsilon/\partial N$ observed at this stage.

The second stage can be characterise by a constant $\partial\varepsilon/\partial N$ value (see Figure 4 and Figure 8, in which a constant slope $\partial\varepsilon/\partial N$ has been pointed at stage II). Table 1 reproduces the $(\partial\varepsilon/\partial N)_{II}$ values at stage II in

relation with the maximum applied load, as it is the maximum strain at each cycle the critical variable to establish the mechanisms changes.

Table 1: $(\partial\varepsilon/\partial N)_{II}$ VALUES

σ_{max} in of (%)σ_r	$(\partial\varepsilon/\partial N)_{II}$ (cycle^{-1})
90	$20.52\cdot10^{-5}$
80	$14.91\cdot10^{-5}$
70	$64.36\cdot10^{-6}$
60	$19.04\cdot10^{-6}$
50	$34.91\cdot10^{-6}$
40	$11.48\cdot10^{-6}$

Representing the parameter previously obtained $(\partial\varepsilon/\partial N)_{II}$ as a function of the number of cycles for which fracture happens (N_F), for each stress level, in a double logarithmic scale a failure diagram is stated which assess the material´s fatigue failure through a linear fit as it is indicated in the graph of Figure 10. Plotting on the same graph, for each stress level, the corresponding points to the critical number of cycles for which the first and the second transition take place and leads to material´s instability (N_{I-II} and N_{II-III}), it can be checked that linear behaviours are obtained again, limiting the material´s fatigue life.

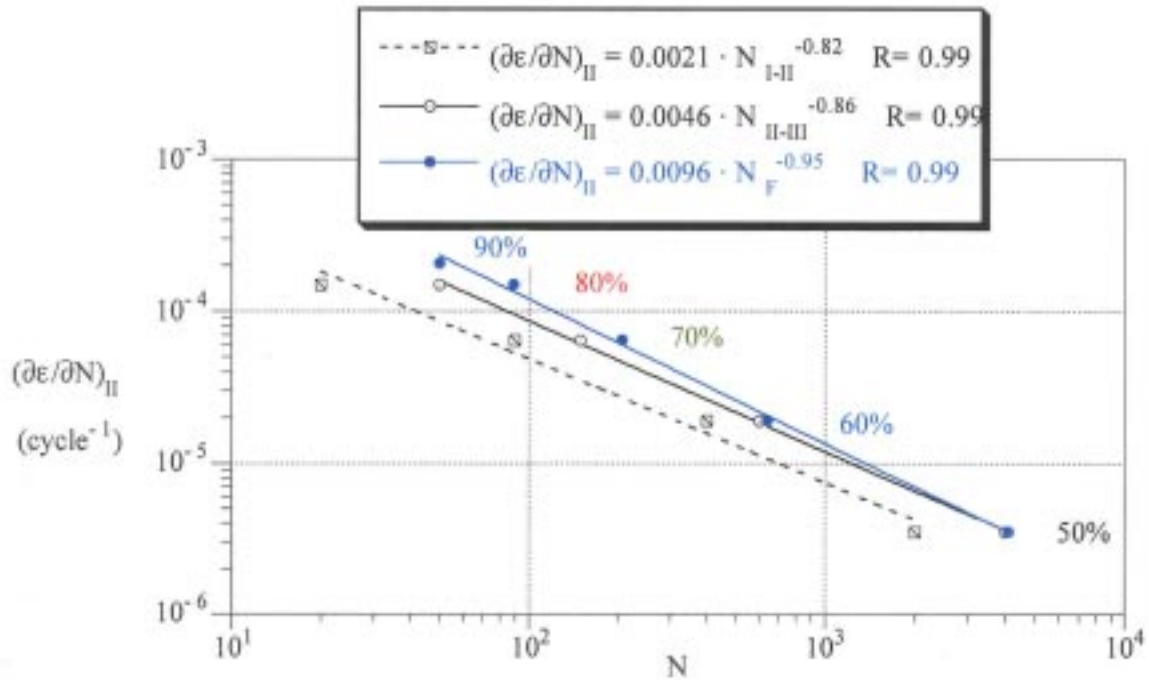

Figure 10: $(\partial\varepsilon/\partial N)_{II} = (\partial\varepsilon/\partial N)_{II}$ (N)

The fits establish that there is an approximately inversely proportional relation between the material´s deformation velocity average at stage II $(\partial\varepsilon/\partial N)_{II}$ and the time or the number of cycles to reach the critical transitions and the fracture conditions. Takahara et al [8] established the fatigue fracture criterion on the basis of average hysteresis energy loss during fatigue process with a similar law for several polymers. Later on they extended this approach to short glass fibre reinforced finding the same linear correlation [9]. It should be reminded that both $\partial\varepsilon/\partial N$ and E_H evolution laws reassembles.

4 CONCLUDING REMARKS

From the work performed it has been established the mechanisms that govern the fatigue behaviour evolution of the fibre glass reinforced PA 6.6 up to the moment of failure. The successive stages involucrated in the fatigue process are produced showing different stages as the next sequence explains:

- Stage I: Initially the material´s fatigue damage is associated exclusively to a creep process which behaviour corresponds to the temperature evolution that depends on the stress level applied.
- Stage II: The maximum material´s strain reached determines at a critical value a transition between stage I and II. For this point there is a dynamic mechanical effect added to that produced by the creep process, producing an homogeneous crazing growth in the material.
- Stage III: Again the maximum material´s strain reaches a second critical value for which a local instability in a particular crazing area takes place, creating a crack growth associated to a high localised strain.
- Fracture: The crack created develops accompanied by a temperature increasement causing a decrease in the material´s strength. Finally the material breaks when the maximum stress applied equals its strength.

As a final result, a failure diagram has been represented on the basis of strain rate during the fatigue process to establish an instability and fracture criterion for the material.

5 REFERENCES

1. TIFSA: *Informe de Instrumentación. Sujeciones de carril P2 y Nabla. Línea de Madrid a Alicante, P. K. 391/330*. Madrid. Septiembre, 1992.
2. Casado, J. A., Gutiérrez-Solana, F., Polanco, J. A. and Kerkhofs, F. *Efecto del tipo de onda en el comportamiento en fatiga de poliamidas reforzadas y de acetales.* Actas I Congreso Nal. de Mat. Comp. Sevilla-95.
3. Casado, J.A., Gutiérrez-Solana, F. and Polanco, J.A. *Waveform and waiting time effects on the fatigue behaviour of reinforced polyamides and acetals.* ECF 11. Mechanics of Damage and Failure (1996). Vol III., pp.1809-1814.
4. Casado, J.; Polanco, J.; Gutiérrez-Solana, F. and Guerra, R. *The characterization of the resistance to lateral impact of the insulating part of the P2 rail fastening.* Third International Conference: "Structures Under Shock and Impact-94". Madrid, June 1994. Proceedings of the Third International Conference: 183-190.
5. UNE 53.280-79. Marzo, 1977. *Determinación de las propiedades en tracción.*
6. S. Suresh. *Fatigue of Materials*. Cambridge Solid State Science Series. Cambridge University Press, 1991.
7. Casado, J. A., Polanco, J. A, Gutiérrez-Solana, F., Carrascal I. and Setién, J. *Parámetros críticos del comportamiento en fatiga de la poliamida 6.6 reforzada con fibra de vidrio corta.* Anales de Mecánica de la fractura. Vol. 16. Torremolinos, Abril-1999.
8. A. Takahara, K. Yamada, T. Kajiyama and M. Takayanagi, *J. Appl. Polym. Sci.*, **25**, 597597 (1980).
9. A. Takahara, T. Magome and T. Kajiyama. *Effect of Glass Fiber-Matrix Polymer Interaction on Fatigue Characteristics of short Glass Fiber-Reinforced Poly(butylene Terephthalate) Based on Dynamic Viscoelastic Measurement During the Fatigue Process. Journal of Polymer Science. Volume 32, number 5. April, 1994.*